Excitation of Airborne Acoustic Surface Modes Driven by a Turbulent Flow

Shishir Damani[*], Eric Totten[†], Laura Davies[†], Nathan Alexander[‡], and William J. Devenport[§]
Virginia Polytechnic Institute and State University, Blacksburg Virginia 24060, United States of America

Benjamin P. Pearce[¶], Samuel R. Shelley[ǀ], Timothy A. Starkey[**], Alastair P. Hibbins[††], and J. Roy Sambles[‡‡]
University of Exeter, Exeter, Devon EX4 4QL, United Kingdom

This experiment demonstrated the generation of trapped acoustic surface waves excited by a turbulent flow source through the coupling of pressure fluctuations at the interface between an acoustic metamaterial and a flow environment. The turbulent flow, which behaves as a stochastic pressure source, was produced using a fully developed turbulent wall jet. The plate in the wall jet was perforated with a single cavity. On the flow-side it was capped by a Kevlar weave to ensure the cavity did not significantly disturb the flow, whilst on the adjacent side the cavity was open to the quiescent (static) environment. The through-cavity opening, on the quiescent side, was flush with an acoustic metasurface waveguide, which, through evanescent diffractive coupling of the pressure field, produced an acoustic surface mode. This acoustic mode was trapped at the plate surface, with its mode dispersion determined by the surface geometry. The results of two different metasurface geometries are discussed; (1) a slotted cavity array, and (2) a meander connected cavity array, each demonstrating a different trapped surface wave dispersion behavior. Fourier transform and correlation analyses of spatially-resolved temporal acoustic signals, measured close to the metamaterial surface, were used to construct the frequency- and wavevector-dependent acoustic mode dispersion. Results demonstrated the flow can indeed be used to excite these acoustic modes and that their mode dispersion can be tailored towards realizing novel control of turbulent flow through acoustic-flow interactions.

I. Introduction

Surface structures can have a significant impact on the pressure fluctuations that manifest above them. In the aerodynamics of turbulent boundary layer flows, surface treatments can cause significant changes to the sound generated from, and pressure fluctuations present within, the flow; experimental studies have examined the impact of roughness [Glegg *et al*. 2009, Devenport *et al*. 2010, Devenport *et al*. 2011] and discontinuous surface features [Catlett *et al.* 2014] using wall jet measurements with a turbulent flow. Various surface topologies have been developed to mitigate these effects, for instance the study of flow generated sound and pressure fluctuations produced by a range

[*]Graduate Student, Kevin T. Crofton Department of Aerospace and Ocean Engineering.
[†]Undergraduate Student, Kevin T. Crofton Department of Aerospace and Ocean Engineering.
[‡]Assistant Professor, Kevin T. Crofton Department of Aerospace and Ocean Engineering. Senior Member AIAA.
[§]Professor, Kevin T. Crofton Department of Aerospace and Ocean Engineering. Associate Fellow AIAA.
[¶]Ph.D. Student, Department of Physics and Astronomy.
[ǀ]Postdoctoral Research Fellow, Department of Physics and Astronomy.
[**]Research Fellow, Department of Physics and Astronomy.
[††]Professor, Department of Physics and Astronomy.
[‡‡]Professor, Department of Physics and Astronomy.

of surface treatments, including ordered roughness fetches [Alexander *et al*. 2013, Alexander *et al.* 2014], bio-inspired canopy structures [Clark *et al*. 2016] and porous surfaces [Alexander *et al*. 2015].

In the field of acoustic metamaterials, structured surfaces or bulk structured materials have been designed to influence the acoustic pressure field for a variety of applications such as acoustic filtering, focusing, and absorption [Assouar *et al*. 2018]. A typical acoustic metasurface comprises sub-wavelength periodic structuring; these can include membranes, resonator cavities, or elastic materials. One type of acoustic wave phenomena that can exist in these types of designer materials are non-radiative waves called Acoustic Surface Waves (ASWs). An example of a geometry that supports Acoustic Surface Waves is a simple one-dimensional rectangular grating of resonator cavities in a solid material [Kelders *et al.* 1998]. The pressure field is highly localized at the interface, and decays exponentially in the direction of the surface normal. The diffractive coupling of the pressure field between resonator cavities results in a mode of the system that begins at zero-frequency that disperses, with in-plane wavevector, $k_{||,}$ toward the resonance frequency of the cavity array. These modes are interesting because their group velocities and dispersion relations can be manipulated by modifying the structure.

This paper presents results that bring together turbulent flow and acoustic metasurfaces. Experimental results demonstrating the excitation of acoustic modes on periodic-structured surfaces that are driven by pressure fluctuations from a turbulent source are shown.

II. Acoustic metamaterial geometries

The metamaterial geometries studied were periodic-cavity-array waveguides in an acoustically rigid material that guide sound in one dimension along the surface. The first sample, termed the 'slot array', was an array of open slots that extended in the spanwise direction, was periodic in the streamwise direction (relative to the flow) and had depth into the solid material. The second surface, the 'meander array', was a continuous open slot that meanders the length of the sample in the streamwise direction. Figure 1(a) and (b) display schematic diagrams and dimensions of both samples. Similar metasurface geometries have been studied in the literature with acoustic excitation and detection [Beadle *et al.* 2019, Ward *et al.* 2019].

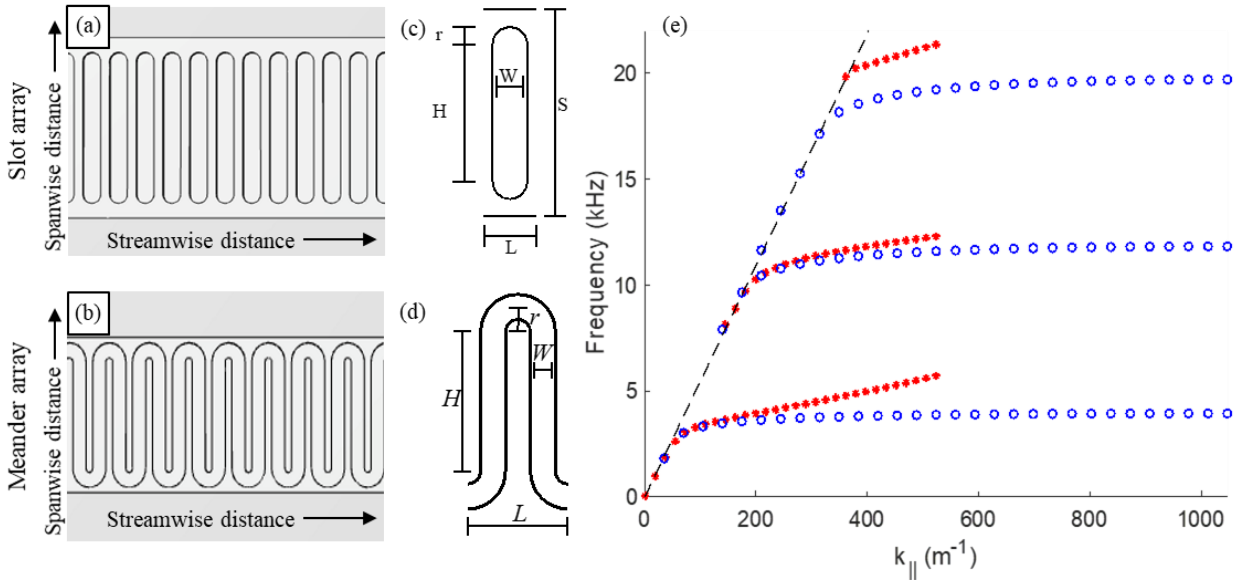

Figure 1: Schematics of the slot array and meander structure: (a) and (b) display schematics, (c) and (d) show the associated unit cells for each structure. (e) calculated dispersion from numerical simulations showing the predicted mode shapes for the slot array (blue circles) and meander structure (red stars). Data is shown in the first Brillouin zone for positive in-plane wavevector. The difference in wavevector at the Brillouin zone boundary is due to the different unit cell dimensions. The dimensions for the slot array design are: r = 1 mm, H = 15 mm, W = 2 mm, L = 3 mm, S = 20 mm. The dimensions for the meander array design are: r =1.5 mm, H = 14 mm, W = 2 mm, L = 6 mm. Both arrays have depth D = 21.4 mm into the page.

The acoustic surface wave mode dispersion for both samples was numerically calculated using Finite Element Method (FEM) simulations and is presented in Figure 1(e). The dashed line indicates the 'sound line', which is the dispersion of a free-space acoustic wave travelling parallel to the sample surface, given by $k_0 = 2\pi f/c$, where k_0, f and c, are the wavevector, frequency, and velocity of the free space wave, respectively. The eigenfrequency solutions plotted in Figure 1(e) indicate that both samples support trapped acoustic modes. Since the simulated surface mode dispersion relation exists with wavevector magnitude that exceeds that of the free-space sound line, their momentum is too large to match to free-space radiation.

The first order mode of the slot array (Figure 1(e) blue circles) begins at zero frequency, travels up the sound line, before strongly dispersing to a resonant frequency at the first Brillouin zone boundary ($k_{BZ} = \pi/2L$). This resonant frequency is strongly dictated by the 1st volumetric resonance in the cavity. Here this corresponds to a quarter-wave resonance in the cavity depth ($\lambda/4$). The two modes shown at higher frequency asymptote correspond to multiples of this cavity depth resonance, i.e. $n\lambda/4$, where $n = 3, 5$. Note that as this mode disperses toward the Brillouin zone boundary, the group velocity, v_g, ($= d\omega/dk$, where ω denotes angular frequency) approaches zero.

The surface mode dispersion of the meander sample (Figure 1(e) red stars) shows different behavior compared to the slot array. The surface mode leaves the sound line and exhibits a linear dispersion with constant group velocity. This is attributed to the interplay between waveguide-like and isolated resonator-like dispersion (like the slotted array), which arises in this connected meander-line channel. The dispersion relation in this system can be described by a waveguide term ($k_{||}$), and a depth (k_z) resonance term (see Beadle *et al*. for further discussion) by:

$$f = \frac{c}{2\pi}\sqrt{\left(\frac{k_{||}}{n_{wg}}\right)^2 + k_z^2}.$$

Here c is the speed of sound and n_{wg} is the ratio of the meander path length to the unit cell pitch. At low $k_{||}$ values the depth resonance term dominates so the mode behaves similarly to the slot array, travelling up the sound line before dispersing away. However, as the value of $k_{||}$ increases the waveguide term becomes dominant. This term has no limit so changes continuously with $k_{||}$. This results in a mode that tends to a straight line with a near constant group velocity, much less than the speed of sound in air. The other key difference from the slot array is that the surface mode does not approach the Brillouin zone asymptotically, this arises due to the glide symmetry of the surface geometry and causes the mode to pass through the first Brillouin zone boundary without being perturbed.

Using the numerical model, it was established that an acoustic surface mode solution exists for two waveguide-like metasurfaces. To establish their existence with a wholly acoustics measurement, acoustic excitation and acoustic detection, a deterministic measurement would be used. A loudspeaker source would be placed close to the sample surface, it would emit a sound pulse, and the pressure field of the surface mode would be measured as a function of time and distance in the propagation direction. Fourier analysis of this measurement would produce the dispersion of the surface mode. To establish the surface mode existence using a turbulent flow excitation, an analogous experiment was performed in a wind tunnel with two critical differences: (1) the flow was introduced to the metasurface through an open-through-cavity topped with Kevlar weave on the flow side, and (2) a pair of microphones were used to characterize the surface mode pressure field – one provided a fixed reference, and the other traversed in the wave propagation direction.

The open-through-cavity, from the flow to the quiescent side, was twice the cavity depth, and was positioned at the center of the waveguide sample. Figure 2 shows a schematic of this slot, from the flow, and from the quiescent side. On the flowside, Kevlar, which is assumed to be transparent to the pressure fluctuations, was placed over the sample surface to ensure the wall jet surface remains smooth. On the quiescent side, the cavity opens into a cavity on the metasurface side. Figure 3 displays a schematic cross-section through the metasurface to further illustrate the through-cavity geometry and shows the location of the fixed microphone and the direction of traverse for the moving microphone in the experiment.

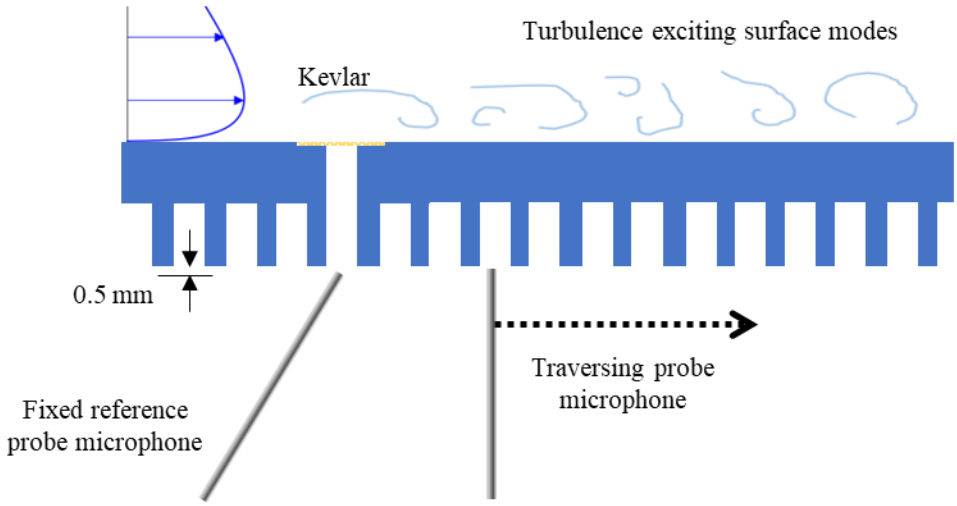

Figure 2: Schematic of hole, from the flow and quiescent side.

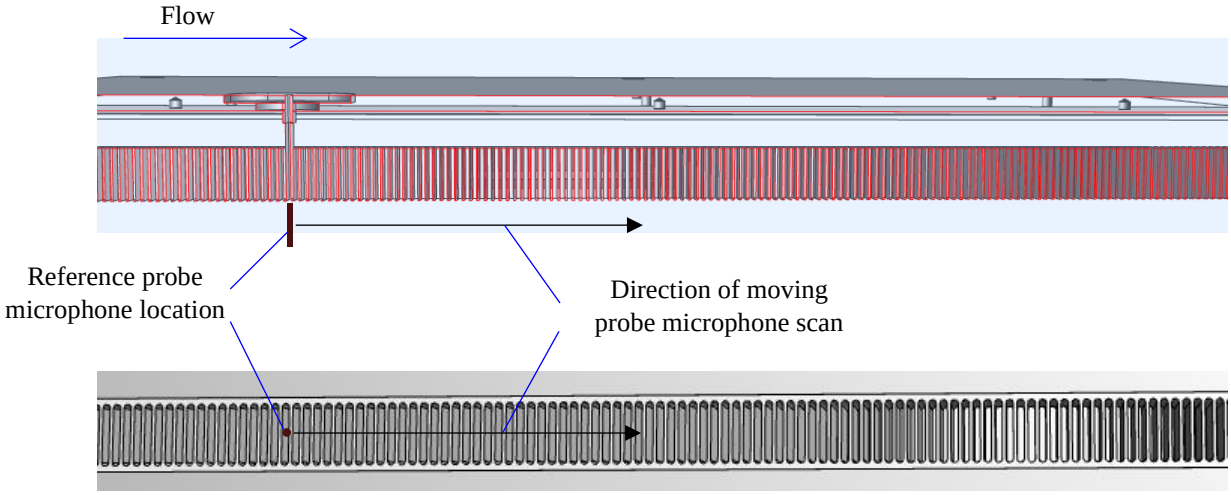

Figure 3: *Top:* Streamwise cross section through the slot metasurface, *Bottom:* view from underneath, showing the location of the reference and moving probe microphones for the measurements presented.

III. Apparatus and Instrumentation

A. Wall Jet Wind Tunnel

This study was conducted in the Virginia Tech Anechoic Wall Jet Tunnel shown in Figure 4. The tunnel uses a Cincinnati Fan model which produces a maximum flow rate of 0.945 m^3s^{-1} and is equipped with SSA-8 steel discharge silencer to reduce noise by 5 to 10 dB. The flow exits the silencer and passes through a flexible hose into an anechoically treated settling chamber. This flexible hose mechanically isolates the blower from the rest of the tunnel. The settling chamber is lined with 101.6 mm acoustic pyramid foam with an absorption coefficient of 0.75 at 2000 Hz and 0.96 at 4000 Hz. It also has a series of baffles which block direct noise radiation through to the nozzle. After the settling chamber, the flow passes through a 2D contraction and out over a large plate, 3048 mm long 1524 mm wide and 9.525 mm thick, via a nozzle which is 12.7 mm tall and 1219 mm wide. Further description of the settling chamber and contraction is given in Kleinfelter *et al.* 2019. The plate is made of Aluminum 6061-T651 and sits in an anechoic chamber. The bottom surface of the test plate is at a height of 1333.5 mm above the ground supported by a 3-piece steel frame. The anechoic chamber is 4.718 m long, 3.238 m wide, and 2.744 m tall, made with an aluminum skeleton lined with MDF boards for sound insulation. The inside of the anechoic chamber is covered with 101.6 mm acoustic wedge foam and 152.4 mm square bass corner foam. The end of the test plate has a curved edge for a Coanda effect. The maximum flow speed at the nozzle, U_j was 70 ms^{-1}. At the location of the through cavity, the maximum

velocity U_m of the boundary layer profile was 24.3 ms^{-1}. From Figure 5(a), it can be confirmed that the flow lied within the turbulent regime. The profile is shown normalized on maximum velocity and the quantity $y_{1/2}$, which is defined as the vertical distance from the wall to the point where the local velocity decays to half the maximum value in the outer region of the boundary layer. Re_j is the Reynolds number based on jet velocity and nozzle height, Re_x is the Reynolds number based on jet velocity and distance to the measurement location, h is the nozzle height, δ is the boundary layer thickness and δ^* is the displacement thickness. Numerical values for the boundary layer properties are given in Figure 5. The wall-jet tunnel speed, temperature, settling chamber pressure, and static pressure were monitored and recorded with an NI DAQ USB-6211. The static pressure and temperature sensors were placed just outside of the nozzle exit inside the anechoic chamber.

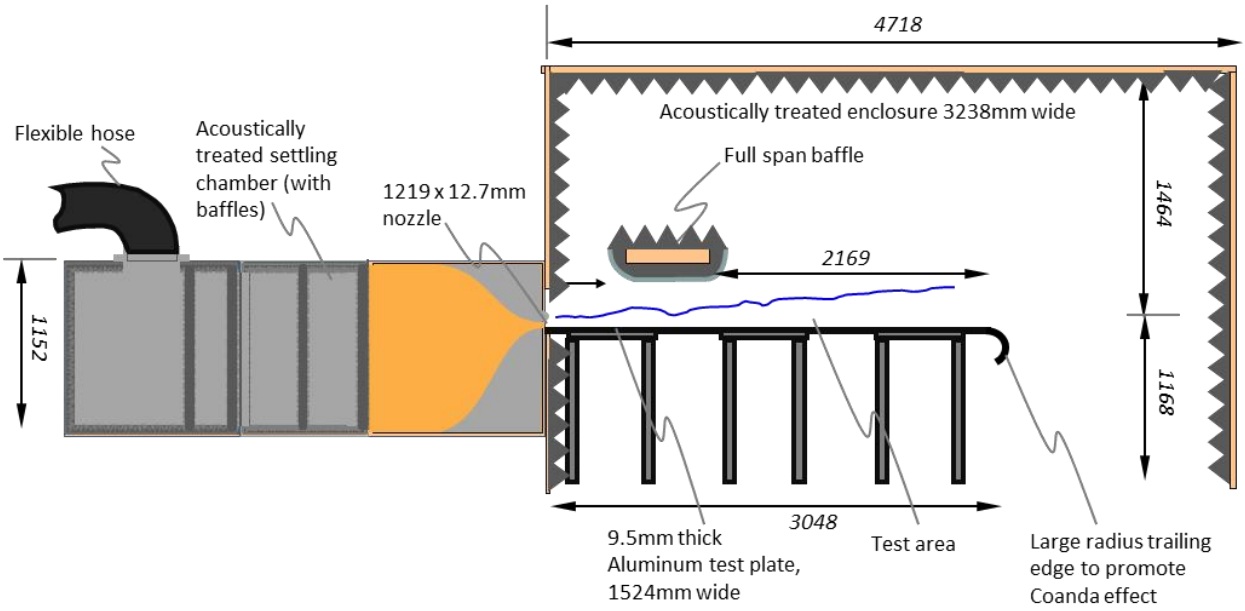

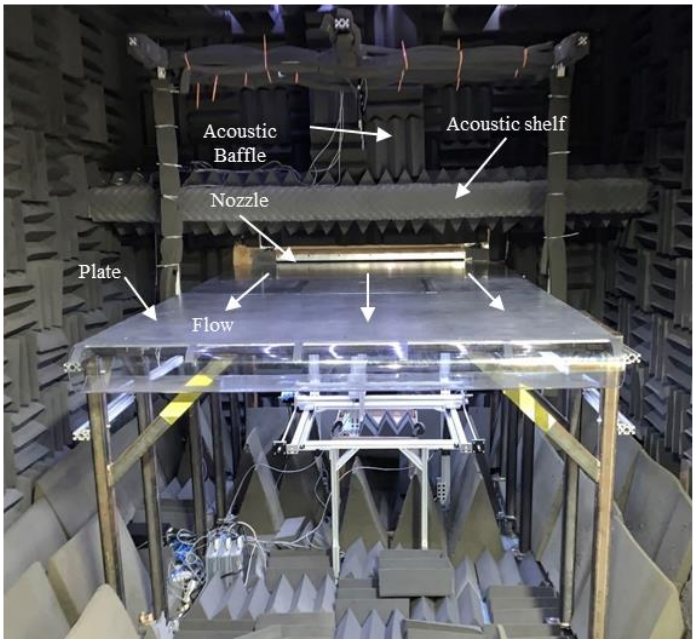

Figure 4: *Top:* Schematic diagram of Virginia Tech Wall-Jet Tunnel. *Bottom:* View from the downstream end of the test plate of the experimental rig.

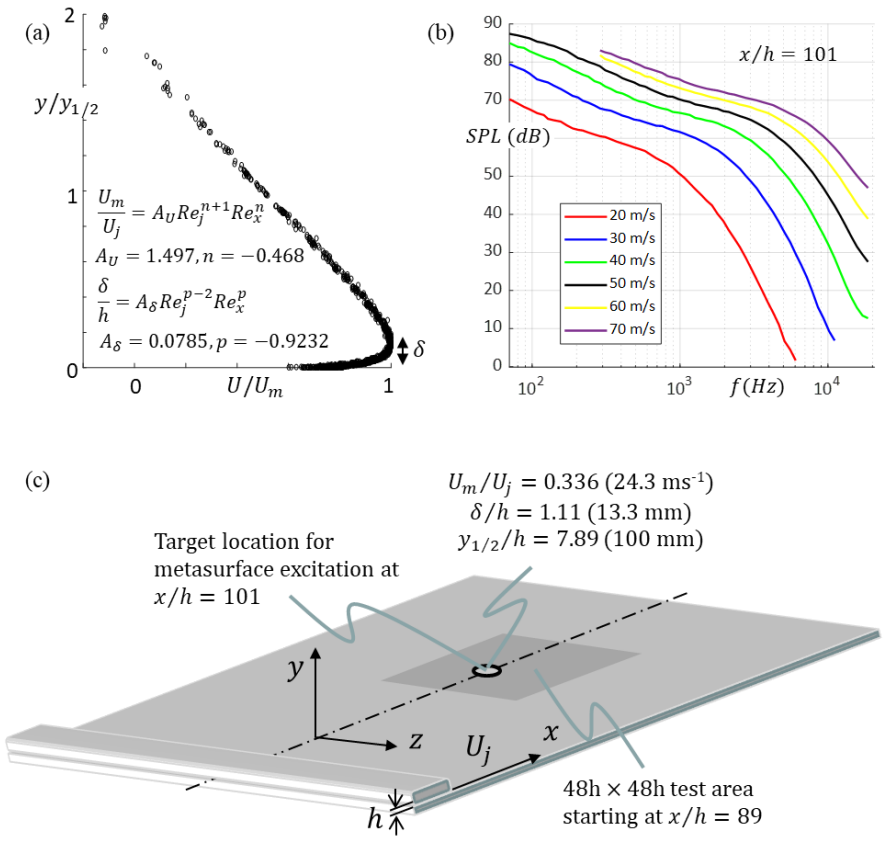

Figure 5: Flow characteristics over the through cavity location: (a) Boundary layer velocity profile in the wall normal direction, (b) Wall pressure spectrum at various speeds, (c) Boundary layer properties at the through cavity location. The parameters are as follows: $h = 12.7$ mm, $x = 1282.7$ mm, $Re_j = 54900$, $Re_x = 5550000$, $M = 0.071$, $y_{1/2} = 100$ mm, $\delta = 13.3$ mm, $\delta^* = 0.831$ mm [Kleinfelter *et al.* 2019].

B. Metasurface Fabrication and Mounting

The metasurfaces used in this study were manufactured using a Stratasys Connex3 3D printer. The Connex3 printer uses Digital ABS Plus with a layer thickness of 16 microns. The length of each metasurface was 609.6 mm in the flow

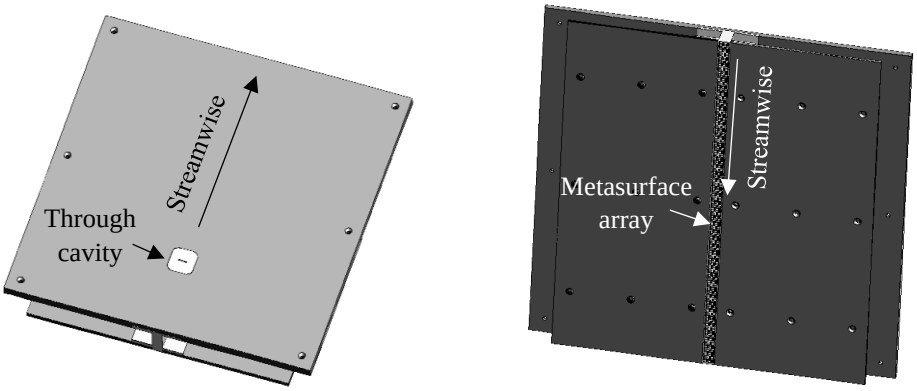

Figure 6: 3D schematics of the test plate mount for metasurface sample, Left: top side of the metasurface., Right: showing the bottom side of the assembled metasurface.

direction. The width of the entire fabricated structure was 520.7 mm on the underside of the wall-jet flow plate which includes large aluminum side plates flanking the metasurfaces in the spanwise direction (shown in Figure 6). The end of the metasurface closest to the nozzle exit was located at 1130.3 mm from the exit and the through cavity was located 152.4 mm further downstream. The entire structure of each metasurface was made of 3 aluminum plates and the 3D printed structure. The top aluminum plate (609.6 mm long, 609.6 mm wide, 9.525 mm thick) had a hole that was covered with a small 3D printed disc with a hole of the shape of the through cavity. A Kevlar membrane covered the open hole on the flow side which minimized the flow side disruption of the boundary layer but allowed the cavity to respond to pressure fluctuations on the flow (top) side of the surface. Two-aluminum plates flanking the metasurfaces on the bottom side of the surface were identical with dimensions 609.6 mm long, 250.19 mm wide and 4.064 mm thick. The top and bottom plates were separated by 12 aluminum spacers of length 6.35 mm. The bottom plates were screwed to the 3D printed part with 3 bolts and nuts on each side. An illustration of a metasurface design with side plates is shown in Figure 6. The bottom side of the surface had a smaller width than the top side as this entire structure rested on a provision made in the test plate. The top plate was screwed to an aluminum frame manufactured using 80/20 Inc. extrusions under the test plate and taped neatly to prevent any disruption to the flow above.

C. Instrumentation, Measurements and Analysis

Two Brüel & Kjær Type 4182 probe microphones with 100 mm tube lengths and a sensitivity at 250 Hz of -50 dB ± 3 dB re 1V/Pa, were used to record pressure fluctuations. These microphones had a flat frequency response from 1 Hz to 500 Hz. The microphones were calibrated using a B&K Type 4228 Pistonphone calibrator. One of the microphones was placed under the through cavity (1282.7 mm away from the nozzle exit) of the metasurface at an angle as shown in Figure 7. This microphone was fixed while the other was mounted on a two-dimensional traverse and moved along the metasurface in the streamwise direction or spanwise direction. The traverse used three PDX13 Series Drive with a resolution of 4000 steps per revolution to move the traversing microphone in the streamwise and spanwise direction. The tips of the probes were approximately 0.512 mm from the surface while scanning across the metasurfaces. At each spatial scan point the microphone data was recorded for 8 seconds. Recorded data was then analyzed using fast-Fourier transform analysis and correlation techniques were used to compare the signals measured at each microphone. Additional scans were also made to show the modal structure of the acoustic surface waves formed across the span of metasurfaces. The mode dispersion (as a function of the streamwise in-plane wavevector vs. frequency) was obtained by spatial fast-Fourier transform of the normalized frequency spectra, following a spatial mirror function to remove artifacts associated with a Fourier transform of a positive-only streamwise measurement.

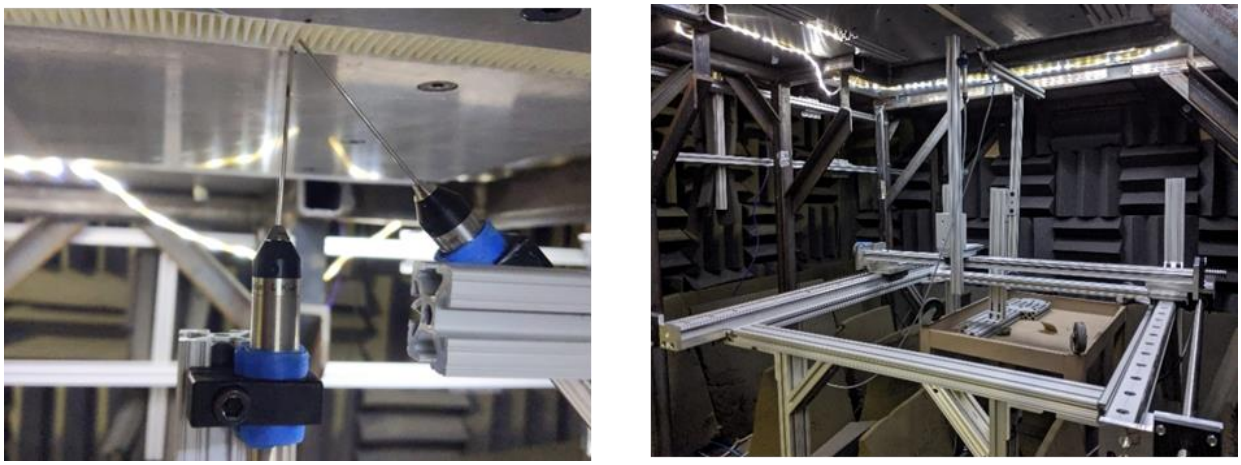

Figure 7: *Left:* Photograph showing the two microphones just under the through cavity (Left mic is the traversing one). *Right:* Traverse under the test plate with the two microphones.

D. Acoustic Numerical Simulations

Numerical simulations of the mode dispersion were performed using COMSOL Multiphysics 5.4a, using the pressure acoustics frequency domain module. In the simulations, the metasurface was described by a single unit-cell

with periodic boundary conditions to represent a waveguide with infinite extent in one dimension. The mode domain above the sample was bounded by a perfectly-matched-layer to approximate the air above to be an infinite half-space. The model assumed the air was an ideal gas without loss and that the sample geometry was an acoustically rigid solid. The software solved an eigenvalue problem to obtain the eigenfrequencies for a given in-plane wavevector.

IV. Results and Discussion

Figure 3 shows schematically the location of the microphone probes during the streamwise traverses. One probe microphone was positioned 0.5 mm below the undersurface of the structure centered on the exit of the through cavity connecting the metasurface to the flow. The second probe was also positioned just below the surface but at a series of positions displaced from the reference microphone in the streamwise direction, following the metasurface centerline. Measurements were made over a dense series of positions (spatial resolution of 0.45 mm) covering a microphone separation from 0 to 150 mm. Figure 3 shows these positions for the slot metasurface, but an identical arrangement was used with the meander metasurface.

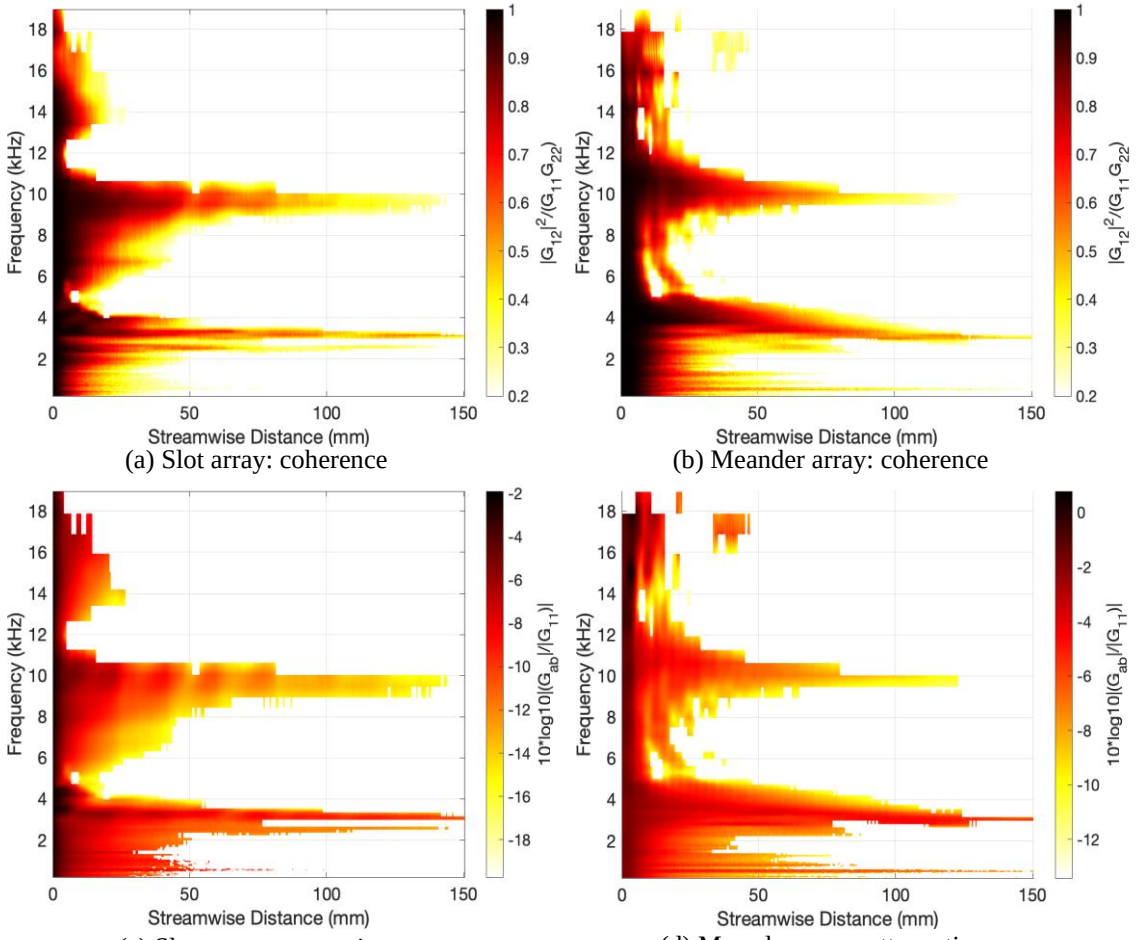

(a) Slot array: coherence (b) Meander array: coherence

(c) Slot array: attenuation (d) Meander array: attenuation

Figure 8: Spectral coherence and attenuation maps as function of frequency and streamwise distance along the metasurface array.

Figure 8 shows results from the microphone scans, made for a wall jet exit velocity of 70 ms^{-1}, corresponding to a maximum local edge velocity in the wall jet boundary layer of 24.3 ms^{-1} ($Re_j = 54900$, $Re_x = 5550000$, $M = 0.071$, $\delta = 13.3$ mm and $y_{1/2} = 100$ mm) at the through cavity location. The flow over the through cavity location is two-dimensional in the time averaged sense and extends about 900 mm wide which is about 53 times the slot width. Figure 8(a) and (b) show coherence spectra between the pressure fluctuations recorded by the reference and moving

probes, for the slotted and meander metasurfaces, respectively. Note that Figure 8 (a) and (b) display data above a minimum significant coherence of 0.2. With both metasurfaces, the rate of decay of coherence with streamwise distance is a strong function of frequency. Significant coherence is sustained over the largest distances, up to 150 mm, at frequencies near the natural depth resonance of the half cavities forming the bulk of the array, around 3.9 kHz for the quarter wave resonance, and 11.8 kHz for the three-quarter wave resonance. Below and between these frequencies the coherence between the pressure fluctuations decays more rapidly and in a form that reflects the varying strength of the acoustic surface waves generated with frequency. It is important to bear in mind that the longitudinal correlation length of the turbulent pressure fluctuations exciting these waves is expected to only be a few millimeters, i.e. a few times the boundary layer displacement thickness [Blake *et al.* 1970].

The strengths of these waves are to some extent revealed in Figure 8(c) and (d) that show the attenuation of the coherent pressure fluctuations. Specifically, the magnitude of the cross-spectrum between the pressure fluctuations sensed by the two probes, normalized on the autospectrum of fluctuations at the reference probe are plotted here in decibels. The attenuation map is, overall, very similar to the coherence maps discussed above. At the fundamental resonant frequency, the attenuation is only 5 dB demonstrating the ability of the metasurface to trap, sustain, and guide an ASW generated by turbulent pressure fluctuations in the wall boundary layer whereas at other modes, the attenuation over the 150 mm of the scan is between 10 and 15 dB. Attenuation occurs because of viscous dissipation of the acoustic fluctuations within the metasurface structure since the waves cannot radiate away from the surface.

Dispersion maps inferred from these scans are shown Figure 9(a) and (b), where they are compared with COMSOL predictions. The dispersion maps are obtained by taking the wavenumber transform of the normalized cross-spectrum between the two probes as a function of probe separation. For the slotted metasurface (Figure 9(a)), the measurements reveal strong ridges peeling off the sound line at frequencies just below those of the depth-resonances of the cavities, at about 3.9, 11.8 and 19.6 kHz. These curved paths are symptomatic of the lower phase and group velocities associated with the acoustic surface waves, and rapidly asymptote to horizontal lines associated with standing wave formation in the cavity. The measurements show significant energy in the acoustic surface waves only to wavenumbers where their group velocity is still significant. The numerical calculations agree well with the measured dispersion curves.

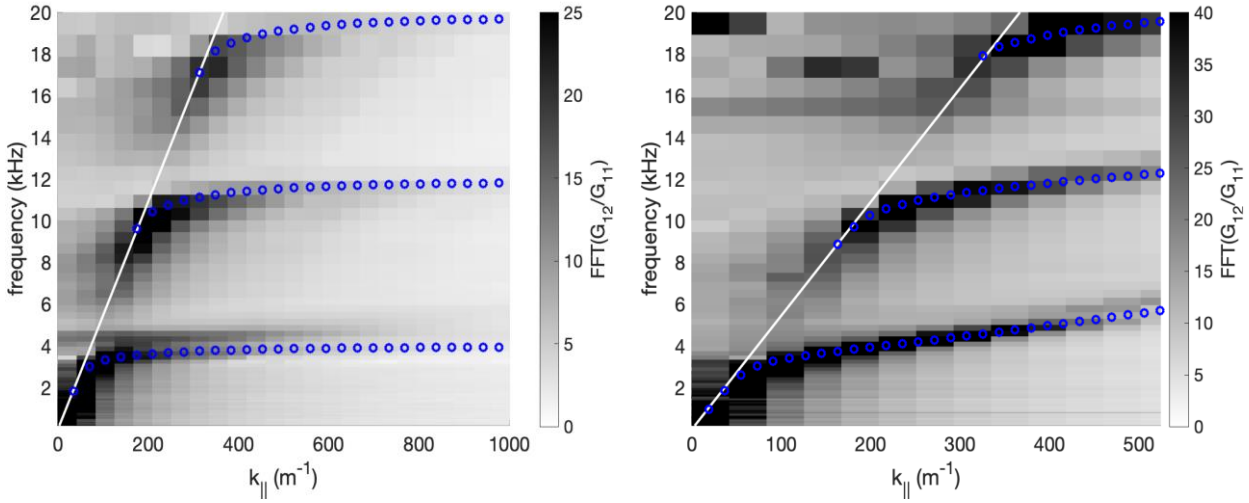

Figure 9: Dispersion maps for (a) slot and (b) meander metasurface arrays. Solid white line indicates the sound line - the dispersion of a free space acoustic wave.

For the meander metasurface, Figure 9(b), the dispersion diagram appears superficially similar but are different in critical details. The meander structure results in acoustic surface waves that remain stronger to much higher wavenumbers and dispersion curves that do not flatten out i.e. near zero group velocity since the acoustic surface waves do not devolve into standing waves at higher wavenumber. The net effect is the generation of much more

intense acoustic surface waves at low speed. Figure 9(b) shows the formation of significant acoustic surface waves with group speeds as low as 1/10th of the sound speed, as indicated by the gradient.

Measurements were also conducted to look at the spanwise structure of the acoustic surface waves for the slot array. For these measurements the reference probe microphone was placed just below the center of the exit of the through cavity, while the second microphone was traversed spanwise across the exit of the through cavity, as well as those of the first and eighth cavities downstream of this position. The turbulent pressure field of the wall jet is expected to have a spanwise coherence length much shorter than the spanwise slot width which means that the flow across the through cavity could be visualized as a superposition of multiple excitation sources at different spanwise stations at an instant of time which would presumably produce a varying output along the slot. Results are plotted in Figure 10 in terms of the coherence between pressure fluctuations sensed by the reference and traversed probe for the 3 slots studied. The horizontal axis shows distance between the probes in the spanwise direction with respect to the middle of the slot, the measurement covering over 94% of the slot width with a spatial resolution of 0.3 mm. The vertical axis shows frequency and the coherence level is represented in contour color. For the through cavity, and the first slot, the coherence of the pressure fluctuations across the span of the slot is almost perfect up to 10 kHz with coherence greater than 0.9 for the through cavity and 0.75 for the first slot. This shows that the through cavity resonator works as a near perfect spanwise averager of the turbulent pressure field to which it is subject. Above 10 kHz, the coherence decays with spanwise separation which is likely because spanwise modes come into play at frequencies higher than 10 kHz with 10.5 kHz corresponding to the frequency of the fundamental spanwise mode. For the 8th slot, the coherence is generally somewhat lower except at the resonant modes i.e. 3.9 and 11.8 kHz. This can be understood from Figure 8, as the ASW communicated pressure fluctuations couple with the metasurface, these remain significant at this distance for resonant modes while other frequencies are attenuated within small distances.

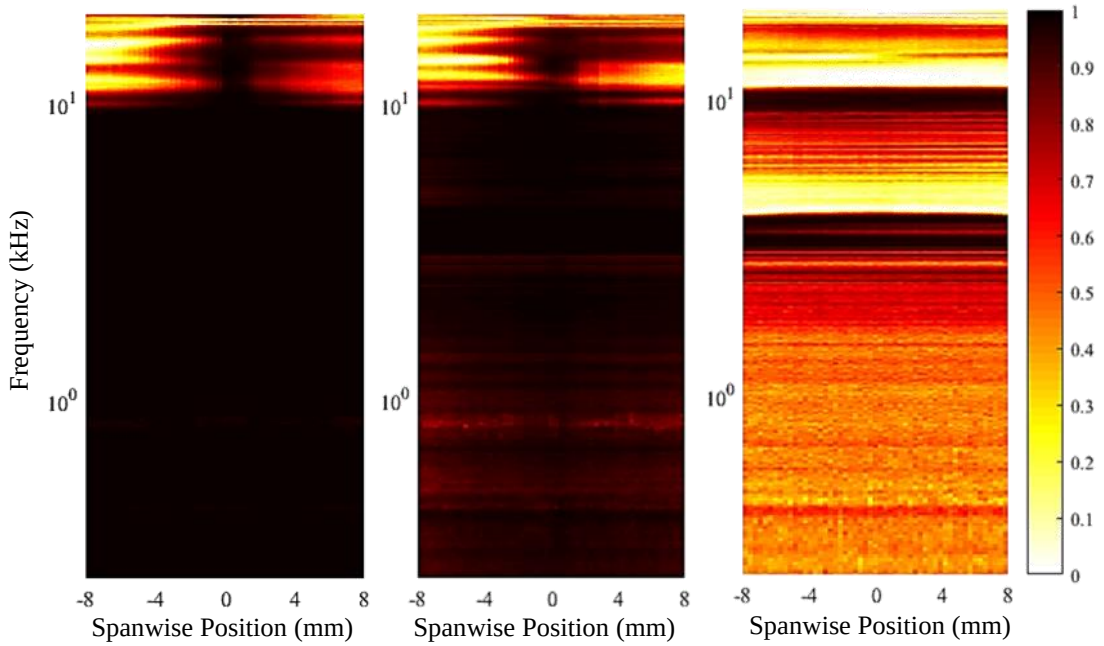

Figure 10: Spanwise coherence at three streamwise locations: (a) through cavity, (b) 1st slot, (c) 8th slot. The streamwise distance between the probes is 0, 3 and 24 mm respectively, these representing the distances between the slots and the through cavity. Note the negative distance refers to the left of the center of the slot when seen against flow direction.

V. Conclusions

In conclusion, we experimentally demonstrate the excitation of an Acoustic Surface Wave (ASW) by a stochastic pressure field generated by a turbulent flow. Results show that a bound acoustic mode is supported by a

structured metasurface placed in the quiescent environment on the underside of a wall jet. The pressure fluctuations from the upper surface were coupled to the ASW through one Kevlar covered slot flush with the wall jet test bed. This through cavity is twice as deep as the metasurface slots which support the ASW, so they have the same depth dictated resonant frequency. While a simple line of slots on the lower surface supports an ASW it is seen that it is difficult to control the velocity of the ASW so that it is comparable to the speed of propagation of the pressure fluctuations on the upper surface. In order to tailor the mode phase and group velocities, a meander groove structure was also investigated, and the surface wave speed was shown to be greatly reduced.

Analysis of the coherence of the surface wave along the sample geometry demonstrated the acoustic mode was indeed bound and coherent over a length scale significantly longer than typical coherence length scales of a turbulent flow. The attenuation of the ASW on both geometries studied indicates a small acoustic loss over the measured propagation distances recorded before the coherence dropped below the value of significant coherence. Spanwise measurements show near-perfect coherence of pressure fluctuations on the underside of the through cavity at frequencies below which spanwise acoustic modes are possible, suggesting that this resonator is a near perfect spanwise averager of the turbulent pressure field to which it is subject. The ASW retains this property at frequencies near resonance as it propagates along the metasurface.

These results are of practical importance as the metasurface is drawing power from the flow at low spanwise wave numbers, precisely the component of the pressure fluctuations responsible for edge noise. Future studies will involve new metasurfaces with a tailored group velocity to far better match the convection speed of the pressure fluctuations over a wide frequency band to create stronger interactions between the ASW and the flow fluctuations. This will ultimately lead to the potential to not only remove energy from the fluctuations but also to inject energy at specific frequencies.

Acknowledgments

The authors would like to thank the Office of Naval Research, in particular Drs. Gregory Orris and Mark Spector, for their support under grant N00014-18-1-2179. Authors at University of Exeter would like to thank the Defence, Science and Technology Laboratory (Dstl), and the Engineering and Physical Sciences Research Council (EPSRC) for their financial support, through which SRS and BPP were supported via the EPSRC Centre of Doctoral Training in Metamaterials (Grant No. EP/L015331/1). We would also like to thank Dr. John D. Smith (Dstl) for encouraging this collaboration and for many useful discussions.

References

Alexander, W.N., Devenport, W.J., and Glegg, S.A.L., "Predictions of Sound from Rough Wall Boundary Layers," *AIAA Journal*, Vol. 51, No. 2, 2013, pp. 465-475.

Alexander, W.N., Devenport, W.J., and Glegg, S.A.L., "Predictive Limits of Acoustic Diffraction Theory for Rough Wall Flows," *AIAA Journal*, Vol. 52, No. 3, 2014, pp. 634-642.

Alexander, N. and Devenport, W. "Noise Produced by Fabric and Wire Mesh Covered Panels in Low-Speed Anechoic Wind Tunnels," AIAA 2015-3261, June 2015.

Assouar, B., Liang, B., Wu, Y., Li, Y., Cheng, J.-C., and Jing, Y., "Acoustic metasurfaces," *Nature Review Materials*, Vol. 3, No. 12, 2018, pp. 460–472.

Beadle, J. G., Hooper, I. R., Sambles, J. R., and Hibbins, A. P., "Broadband, slow sound on a glide-symmetric meander-channel surface," *The Journal of the Acoustical Society of America*, Vol. 145, No. 5, 2019, pp. 3190–3194. https://doi.org/10.1121/1.5109549

Catlett, M., Devenport, W. J., and Glegg, S., "Sound from boundary layer flow over steps and gaps," *Journal of Sound and Vibration*, Vol. 333, 2014, pp. 4170-4186.

Clark, I.A., Daly, C.A., Devenport, W., Alexander, W.N., Peake, N., Jaworski, J.W., Glegg, S., "Bio-inspired canopies for the reduction of roughness noise," *Journal of Sound and Vibration*, Vol. 385, 2016, pp. 33-54.

Devenport, W., E. A. Wahl, S. A. L. Glegg, W. N. Alexander and D. L. Grissom (2010). "Measuring surface pressure with far field acoustics," *Journal of Sound and Vibration*, Vol. 329, No. 19, pp. 3958-3971.

Devenport, W. J., Grissom, D. L., Alexander, W. N., Smith, B. S. and Glegg, S. A. L. (2011). "Measurements of roughness noise," *Journal of Sound and Vibration*, Vol. 330, No. 17, pp. 4250-4273.

Glegg, S., and Devenport, W., "The far-field sound from rough-wall boundary layers," *Proceedings of the Royal Society A: Mathematical, Physical and Engineering Sciences,* Vol. 465, No. 2106, 2009, pp. 1717-1734.

Glegg, S. and Devenport, W., "Measurement, signal processing, and uncertainty," *Aeroacoustics of Low Mach Number Flows*, 1st ed., Academic Press, 2017, pp. 271–298.

Kelders, L., Allard, J. F., and Lauriks, J. F., "Ultrasonic surface waves above rectangular- groove gratings," *Journal of the Acoustical Society of America*, Vol. 103, 1998, pp. 2730-2733.

Kleinfelter, A. W., Repasky, R., Hari, N., Letica, S., Vishwanathan, V., Organski, L., Schwaner, J., Alexander, W. N., and Devenport, W. J. "Development and Calibration of a new Anechoic Wall Jet Wind Tunnel," AIAA 2019-1936, Jan 2019.
https://doi.org/10.2514/6.2019-1936

Ward, G. P., Hibbins, A. P., Sambles, J. R., and Smith, J. D., "The waveguiding of sound using lines of resonant holes," *Scientific Reports*, Vol. 9, No. 1, 2019, p. 11508.
https://doi.org/10.1038/s41598-019-47988-7

Blake, W., "Turbulent boundary-layer wall-pressure fluctuations on smooth and rough walls," *Journal of Fluid Mechanics*, Vol. 44, No. 4, 1970, pp. 637-660.
https://doi:10.1017/S0022112070002069